Clinical Cancer Research

Identification of Resistance Pathways Specific to Malignancy Using Organoid Models of Pancreatic Cancer

Mariano Ponz-Sarvise[1,2], Vincenzo Corbo[1,2], Hervé Tiriac[1,2], Dannielle D. Engle[1,2], Kristopher K. Frese[3], Tobiloba E. Oni[1,2,4], Chang-Il Hwang[1,2], Daniel Öhlund[1,2], Iok In Christine Chio[1,2], Lindsey A. Baker[1,2], Dea Filippini[1,2], Kevin Wright[1,2], Tashinga E. Bapiro[5], Pearl Huang[6], Paul Smith[7], Kenneth H. Yu[1,2,8,9], Duncan I. Jodrell[5,10], Youngkyu Park[1,2], and David A. Tuveson[1,2]

Abstract

Purpose: *KRAS* is mutated in the majority of pancreatic ductal adenocarcinoma. MAPK and PI3K-AKT are primary KRAS effector pathways, but combined MAPK and PI3K inhibition has not been demonstrated to be clinically effective to date. We explore the resistance mechanisms uniquely employed by malignant cells.

Experimental Design: We evaluated the expression and activation of receptor tyrosine kinases in response to combined MEK and AKT inhibition in KPC mice and pancreatic ductal organoids. In addition, we sought to determine the therapeutic efficacy of targeting resistance pathways induced by MEK and AKT inhibition in order to identify malignant-specific vulnerabilities.

Results: Combined MEK and AKT inhibition modestly extended the survival of KPC mice and increased Egfr and ErbB2 phosphorylation levels. Tumor organoids, but not their normal counterparts, exhibited elevated phosphorylation of ERBB2 and ERBB3 after MEK and AKT blockade. A pan-ERBB inhibitor synergized with MEK and AKT blockade in human PDA organoids, whereas this was not observed for the EGFR inhibitor erlotinib. Combined MEK and ERBB inhibitor treatment of human organoid orthotopic xenografts was sufficient to cause tumor regression in short-term intervention studies.

Conclusions: Analyses of normal and tumor pancreatic organoids revealed the importance of ERBB activation during MEK and AKT blockade primarily in the malignant cultures. The lack of ERBB hyperactivation in normal organoids suggests a larger therapeutic index. In our models, pan-ERBB inhibition was synergistic with dual inhibition of MEK and AKT, and the combination of a pan-ERBB inhibitor with MEK antagonists showed the highest activity both *in vitro* and *in vivo*.

Introduction

Pancreatic ductal adenocarcinoma (PDA) is a deadly disease with a 5-year survival rate of less than 8% (1). This dismal prognosis results from late diagnoses and limited efficacy of systemic treatments (2). *KRAS* mutation is detected in more than 90% of PDA (3). The majority of mutations are substitutions in codons 12–13 that cause persistent KRAS activation (4). Activated KRAS engages a multitude of pathways that regulate

[1]Cold Spring Harbor Laboratory, Cold Spring Harbor, New York. [2]Lustgarten Pancreatic Cancer Research Laboratory, Cold Spring Harbor, New York. [3]Cancer Research UK Manchester Institute, Manchester, United Kingdom. [4]Graduate Program in Molecular and Cellular Biology, Stony Brook University, Stony Brook, New York. [5]Department of Oncology, University of Cambridge, Cambridge, United Kingdom. [6]Merck & Co., Kenilworth, New Jersey. [7]IMED Biotech Unit, AstraZeneca, Cambridge, United Kingdom. [8]Rubenstein Center for Pancreatic Cancer Research, Memorial Sloan Kettering Cancer Center, New York, New York. [9]Weill Medical College at Cornell University, New York, New York. [10]Cancer Research UK Cambridge Institute, The University of Cambridge, Li Ka Shing Centre, Cambridge, United Kingdom.

Note: Supplementary data for this article are available at Clinical Cancer Research Online (http://clincancerres.aacrjournals.org/).

Current address for M. Ponz-Sarvise: Department of Oncology, Clinica Universidad de Navarra, CIMA, IDISNA, Pamplona, Spain; current address for V. Corbo and D. Filippini: Department of Diagnostics and Public Health, University of Verona, Verona, Italy; current address for C.-I. Hwang: Department of Microbiology and Molecular Genetics, University of California, Davis, California; current address for D. Öhlund: Department of Radiation Sciences and Wallenberg Centre for Molecular Medicine, Umeå University, Umeå, Sweden; current address for I.I.C. Chio: Institute for Cancer Genetics, Columbia University Medical Center, New York, New York; current address for T.E. Bapiro: IMED Biotech Unit, AstraZeneca, Cambridge, United Kingdom; current address for D.D. Engle: The Salk Institute for Biological Studies, La Jolla, California; current address for H. Tiriac: Department of Surgery, University of California, San Diego, La Jolla, California; and current address for P. Huang: Cygnal Therapeutics, Boston, Massachusetts.

M. Ponz-Sarvise, V. Corbo, H. Tiriac, D.D. Engle, and K.K. Frese are co–first authors of this article.

Corresponding Authors: David A. Tuveson, Cold Spring Harbor Laboratory, One Bungtown Road, Cold Spring Harbor, NY 11724. Phone: 516-367-5246; Fax: 516-367-8353; E-mail: dtuveson@cshl.edu; and Youngkyu Park, Phone: 516-367-6856; E-mail: ypark@cshl.edu

Clin Cancer Res 2019;25:6742–55

doi: 10.1158/1078-0432.CCR-19-1398

Translational Relevance

Therapeutic strategies for pancreatic ductal adenocarcinoma (PDA) are largely ineffective. Kras signaling is aberrantly activated but has proven a difficult clinical target. Dual inhibition of the two KRAS effectors, AKT and MAPK, failed in clinical trials due in part to the rapid development of resistance. The KPC mouse model of PDA is resistant to dual MEK and AKT inhibition and activates Egfr and ErbB2 *in vivo*. Using organoids, we explore the differential response of nonneoplastic and PDA cells to MEK and AKT inhibition. Hyperactivation of the ErbB pathway was observed in the neoplastic, but not normal, organoids in response to dual MEK and AKT blockade. Inhibition of MEK and ERBB was synergistic and resulted in tumor regressions in an orthotopic xenograft model. These data suggest that combined inhibition of MEK and ERBB may be able to achieve therapeutic index. Together, these data demonstrate that the three-dimensional organoid culture system is a platform to interrogate the effects of targeted therapies in both neoplastic and nontransformed cells and can complement standard genetically engineered mouse and transplantation models.

cellular processes such as proliferation and cell survival (4). The importance of *KRAS* mutations in PDA tumorigenesis and maintenance has been extensively demonstrated in genetically engineered mouse models (GEMM; refs. 5–7).

Although recent attempts to pharmacologically target KRAS have yielded success in the setting of G12C mutation (8), this mutation is uncommon in pancreatic cancer (9), and KRAS has otherwise proven difficult to target (10). Therefore, alternative approaches have often focused on developing agents that target two downstream effector pathways, the MAPK and the PI3K signaling cascades (10).

However, marginal or no activity has been observed following the combined inhibition of MAPK/ERK and PI3K/AKT pathways in GEMMs (11, 12), xenografts (13, 14), and phase II clinical trials (13, 15). Targeting of MEK and AKT signaling with selumetinib (AZD6244) and MK2206 was tested in KRAS-driven human malignancies in phase I clinical trial (NCT01021748). Among 29 enrolled patients, there was 1 PDA patient who achieved a marginal response, albeit the patient's KRAS status was unknown (13). In addition, dual inhibition of MEK and AKT did not improve overall survival in PDA patients for whom gemcitabine-based chemotherapy had failed in randomized phase II clinical trial (NCT01658943; ref. 15). The existence of complex feedback mechanisms when individually inhibiting MEK or AKT has been reported (16–21) and includes the activation of a number of receptor tyrosine kinases (RTK; including ERBB receptors), explaining the low efficacy of agents targeting these individual pathways in PDA and other malignancies (16–21). Therefore, we sought to better understand the alterations in cellular signaling that occur upon dual MEK and AKT blockade in PDA and to determine whether these responses are found in both normal and malignant ductal cells.

The evaluation of therapeutic efficacy in PDA has often relied on monolayer cultures, which does not support the proliferation of nontransformed, normal pancreatic ductal cells. We sought to determine whether resistance to targeted therapy was a unique property of cancer cells or if this property was a common response to targeting these pathways in ductal cells. To directly compare normal and neoplastic responses to targeted therapy, we developed a three-dimensional organoid model system to propagate pancreatic cells from either neoplastic or nonneoplastic tissues (22, 23). Using the organoid model system, we compared the response of normal and malignant cells to combined MEK and AKT inhibition. Within the same media conditions for both cell types, we identified feedback mechanisms specific to neoplastic cells. A better understanding of how nontransformed cells respond to these targeted agents may help identify therapeutic combinations that are less toxic when administered to patients.

In this study, we investigated the efficacy of the dual inhibition of MEK (selumetinib) and AKT (MK2206) in PDA using *Kras*$^{+/LSL\text{-}G12D}$; *Trp53*$^{+/LSL\text{-}R172H}$; *Pdx1-Cre* (KPC) mice (24) as well as in mouse and human pancreatic organoid and monolayer cultures (22). Herein, we show that both mouse and human PDA-derived organoids recapitulate the modest efficacy of the combined MEK and AKT inhibitor treatment *in vivo*. Increased IGF-1R and INS-R phosphorylation was observed after dual MEK and AKT inhibition in both nontransformed and malignant cells, indicating activation of these RTKs. In contrast, hyperactivation of the ERBB pathway was unique to malignant organoids and was not observed in their normal counterparts. Our study suggests that targeting the ERBB pathway may have fewer side effects than targeting the IGF-1R or INS-R pathways and be able to achieve a higher therapeutic index. Interruption of this feedback loop using a pan-ERBB kinase inhibitor resulted in synergistic suppression of cell viability *in vitro* and tumor regressions *in vivo* when combined with MEK inhibition.

Materials and Methods

Cell culture

Cell lines were derived from our murine KPC tumors and maintained in DMEM (41966029, Invitrogen) with 10% FBS (SH30070.03, HyClone) and Pen/Strep. Protein lysates were obtained using RIPA buffer with protease and phosphatase inhibitors. AZD6244 (ARRY-142886, selumetinib, AstraZeneca) and MK2206 (Merck) were dissolved in DMSO. Gemcitabine (Addenbrookes, Memorial Sloan Kettering Cancer Center) was dissolved in saline, and used as indicated. Cell viability experiments were performed using Cell Titer-Glo (G7570, Promega) according to manufacturer's recommended protocols.

Organoid isolation and culture

Detailed procedures to isolate and propagate mouse and human, normal, and neoplastic pancreatic organoids have been described previously (22, 23). In brief, normal pancreatic mouse ducts were manually picked after enzymatic digestion of pancreas with 0.012% (w/v) collagenase XI (Sigma) and 0.012% (w/v) dispase (GIBCO) in DMEM media containing 1% FBS (GIBCO) and were seeded in growth factor–reduced (GFR) Matrigel (BD). For tumors (mT), bulk tissues were minced and digested overnight with collagenase XI and dispase and embedded in GFR Matrigel. In the case of human primary and metastatic pancreatic tumor organoid cultures (hT), tumor tissue was minced and digested with collagenase II (5 mg/mL, GIBCO) in human complete

medium at 37°C for a maximum of 16 hours. The material was further digested with TrypLE (GIBCO) for 15 minutes at 37°C, and embedded in GFR Matrigel. Normal samples were processed as above, except that the collagenase digestion was done for a maximum of 2 hours in the presence of soybean trypsin inhibitor (1 mg/mL, Sigma).

Animals

Trp53$^{+/LSL\text{-}R172H}$, *Kras*$^{+/LSL\text{-}G12D}$, and *Pdx1-Cre* strains on a C57Bl/6 background were interbred to obtain *Pdx1-Cre; Kras*$^{+/LSL\text{-}G12D;}$ *Trp53*$^{+/LSL\text{-}R172H}$ (KPC) mice (24). C57Bl/6 mice were purchased from the Jackson Laboratory. For human tumor organoid xenograft experiments, immunocompromised [NOD *scid* gamma (NSG), Jax stock number 005557] mice were used. All animal experiments were conducted in accordance with procedures approved by the Institutional Animal Care and Use Committee at Cold Spring Harbor Laboratory and the Home Office license and the Cambridge Research Institute Ethics committee in Cambridge, UK.

Therapeutic experiments with organoids

Neratinib, MK2206, and selumetinib (Selleck) were dissolved in DMSO. The final concentration of DMSO was no higher than 0.2%. The following doses were used for the cytotoxicity assay: neratinib and MK2206: 1 nmol/L, 5 nmol/L, 10 nmol/L, 50 nmol/L, 100 nmol/L, 500 nmol/L, 1 μmol/L, 5 μmol/L, 10 μmol/L, 100 μmol/L; selumetinib: 10 nmol/L, 20 nmol/L, 100 nmol/L, 200 nmol/L, 1 μmol/L, 2 μmol/L, 10 μmol/L, 20 μmol/L, 100 μmol/L, 200 μmol/L. When combinations of drugs were used, the EC_{50} of each drug alone was determined in the organoid lines, and the ratio of the two EC_{50}s was calculated. Dose ranges of each drug were then calculated, keeping this EC_{50} ratio constant (25).

For EC_{50} analysis, organoids were dissociated to single cells by triturating organoids in media through a fire-polished glass pipette, and then by enzymatic dissociation with 2 mg/mL dispase dissolved in TrypLE (Life Technologies) at 37°C, until the organoids appeared as single cells under the microscope (15–45 minutes). Cells were counted and diluted to 10 to 30 cells/μL in a mixture of complete media, Rho Kinase inhibitor Y-27632 (10.5 μmol/L final concentration, Sigma), and GFR Matrigel (10% final concentration). Note that 100 μL of this mixture (1,000–3,000 cells per well) was plated in a 96-well plate (Nunc) previously coated with a bed of GFR Matrigel. Once organoids reformed (between 36 and 48 hours after plating, confirmed by microscopy), drugs were added in 100 μL of media. Ten different doses plus a vehicle control were used for each drug, and five replicate wells were treated with each dose. Seventy-two hours after the addition of the drug, cell viability was measured using a luminescence ATP-based assay (CellTiter-Glo, Promega) and a plate reader (I3, Molecular Devices). The curves shown in the figures and the calculated IC_{50} values for both human and mouse were the result of three biological replicates for each type of organoid.

For signaling pathway analysis, including Western blots, RTK arrays, and qRT-PCR, organoids were seeded as fragments in complete media. After 24 hours, media were changed with media containing 1 μmol/L of the indicated drug or drugs. DMSO was used as vehicle control. Where indicated, organoids were evaluated after 60 hours instead of 72 hours to recover sufficient material for protein analyses.

Therapeutic intervention studies in mice

Detailed information about the study design and tumor monitoring was described previously (26). Briefly, upon detection of a mass during weekly manual palpation, KPC mice were subjected to high-contrast ultrasound imaging using the Vevo 2100 System with a MS250, 13–24 MHz scanhead (Visual Sonics, Inc.). KPC mice with tumor diameters of 5 to 9 mm were randomized and enrolled into the therapeutic intervention studies according to the outlined treatment schedules. NSG mice were surgically implanted with human tumor organoids between 8 and 12 weeks of age. In short, organoids were dissociated into single cells and transplanted into the pancreas in 50 μL of 50% GFR Matrigel. Upon reaching clinical endpoint, the engrafted tumors were passaged into new NSG host pancreata as 2 mm^3 fragments using tissue glue (Vetclose, Henry Schein). Human tumor organoid xenografts, passage 1, were enrolled in therapeutic intervention studies upon reaching greater than 350 mm^3 in size. Selumetinib (AZD6244, ARRY-142886, AstraZeneca) and MK2206 (Merck) were formulated in 0.5% methylcellulose. Mice were administered methylcellulose vehicle, 25 mg/kg selumetinib bidaily, 100 mg/kg MK2206 every other day, and/or 50 mg/kg neratinib daily via oral gavage (13, 27, 28). Gemcitabine was administered intraperitoneally at a dose of 100 mg/kg (29).

Pharmacokinetic analyses

Fresh-frozen tumor samples and cell pellets were processed and analyzed as previously described (30). Briefly, gemcitabine LC-MS/MS was performed on a TSQ Vantage triple stage quadrupole mass spectrometer (Thermo Scientific) fitted with a heated electrospray ionization (HESI-II) probe operated in positive and negative mode at a spray voltage of 2.5 KV, capillary temperature of 150°C. Quantitative data acquisition was done using LC Quan2.5.6 (Thermo Fisher Scientific). MK2206 HPLC-MS/MS was performed at Merck Research Labs.

Histology

Tissues were fixed in 10% neutral-buffered formalin and embedded in paraffin. Sections were subjected to immunohistochemical (IHC) staining using the following primary antibodies: Cleaved caspase 3 (9661, Cell Signaling Technology), phosphohistone H3 (3377, Cell Signaling Technology), and Ki67 (D2H10, Cell Signaling Technology).

Western blot analysis

Organoids were harvested using Cell Recovery Solution (Corning) recovery solution on ice. Organoids were lysed using boiling SDS-lysis buffer [50 mmol/L Tris-HCL (pH 7.4), 2% SDS]. Protein lysates were separated using 4% to 12% Bis-Tris NuPage gels (Life Technologies). Isolation of protein from hN organoids following treatment with MEK and AKT antagonists required time points of 48 hours or less in order to obtain sufficient protein quantities. Western blots were probed with the following antibodies: phospho-ERK1/2 (4370, Cell Signaling Technology), pan-ERK1/2 (4695, Cell Signaling Technology), phospho-Akt (4060, Cell Signaling Technology), pan-Akt (4685, Cell Signaling Technology), phospho-ribosomal S6 (4858, Cell Signaling Technology), S6 Ribosomal Protein (2317, Cell Signaling Technology), pan-EGFR (ab2430, Abcam), phospho-EGFR (3777, Cell Signaling Technology), ERBB2 (4290, Cell Signaling Technology), phospho-ERBB2 (2247, Cell Signaling Technology), ERBB3 (12708, Cell Signaling Technology), phospho-ERBB3 (4791, Cell

Signaling Technology), Heat Shock Protein 90 (07-2174, Millipore or 4874, Cell Signaling Technology), actin (sc-1616, Santa Cruz Biotechnologies), and Kras (sc-30, Santa Cruz Biotechnologies). Loading control for Western blot is Hsp90 unless otherwise indicated.

RTK antibody arrays

Mouse Phospho-RTK Arrays (ARY014, R&D Systems) and Human Phospho-RTK Arrays (ARY001B, R&D Systems) were used. Tumors or organoids were processed according to the manufacturer's recommendations, and 200 μg of lysates from tumors treated for 7 days with Gemcitabine or with MEKi + AKTi + Gemcitabine ($n = 3$ mice per group) were incubated with arrays overnight at 4°C. Multiple exposures were used to determine optimal sensitivity, and films were scanned using transillumination. Data was quantified using ImageJ. For each, phospho-protein fold induction relative to experimental controls was determined

Quantitative reverse transcription PCR

RNA was extracted from cell cultures or freshly isolated tissues using TRIzol (Invitrogen), followed by column-based purification with the PureLink RNA Mini Kit (Ambion). cDNA was synthesized using 1 μg of total RNA and TaqMan Reverse Transcription Reagents (Applied Biosystem). All targets were amplified (40 cycles) using gene-specific Taqman primers and probe sets (Applied Biosystems) on a 7900HT Real time-PCR (Applied Biosystem). Relative gene expression quantification was performed using the ΔΔCt method with the Sequence Detection Systems Software, Version 1.9.1 (Applied Biosystems). Levels of each gene were normalized to *HPRT*, and then levels of genes following treatment were normalized to those of the vehicle control.

Dual-drug combination assay

Organoids were plated in 96-well plates and treated with various concentrations of kinase inhibitors, either alone or in combination for 72 hours. Cell viability was determined as described above. Synergistic effects were determined by using the Chou–Talalay method to calculate the combination index (CI; ref. 25). CIs of <1, 1, and >1 indicate synergism, additive effect, and antagonism, respectively. At least two independent experiments with five replicates were performed.

Statistical analysis

Statistical analysis was performed using GraphPad Prism version 6 (GraphPad). All results are expressed as mean ± SEM unless otherwise indicated. Comparisons between groups were performed with the Student *t* test or with the Mann–Whitney nonparametric *t* test as required. Kaplan–Meier curves and the log-rank test were used to analyze differences in survival time. For the dose–response curves, the luminescence data were first normalized to the vehicle control and then analyzed using nonlinear regression. For the qRT-PCR experiments, the Holm–Sidak method was used to perform multiple t tests at once. Error bars indicate SD of the mean. *, $P < 0.05$; **, $P < 0.01$; and ***, $P < 0.001$ relative to vehicle control by multiple t test with correction for multiple comparisons. For the Western differences were considered significant at $P < 0.05$, and the values presented in the figures are *, $P < 0.05$; **, $P < 0.01$; and ***, $P < 0.001$.

Results

The combined inhibition of MEK and AKT shows modest efficacy in a mouse model of PDA

To determine if the KPC mouse model accurately recapitulated the MEK and AKT inhibitor (MEKi and AKTi, respectively) responses observed in patients and by other investigators, we performed a short-term intervention study (7 days, Supplementary Fig. S1A) of MEKi, AKTi, or both, in the presence or absence of gemcitabine (Gem). Treatment of tumor-bearing KPC mice with MEKi and AKTi effectively attenuated the targeted pathways (Fig. 1A). Compensatory hyperphosphorylation of ERK or AKT was observed upon single-agent treatment with AKTi or MEKi, respectively, but treatment with both inhibitors results in attenuation of both signaling pathways (Fig. 1A). Addition of Gem to these short-term treatment regimens reduced the proliferation status of the tumors, whereas the triple combination of MEKi, AKTi, and Gem significantly induced apoptosis (Fig. 1B and C). These data show that the combination of MEKi and AKTi leads to transient responses.

In a survival study setting, Gem or MEKi monotherapy did not significantly affect tumor growth or survival, whereas AKTi single-agent administration reduced tumor growth but without extension in survival (Fig. 1E; Supplementary Fig. S1B–S1E). However, when Gem was administered in combination with either AKTi or MEKi, there was a substantial decrease in tumor growth compared with vehicle control or Gem monotherapy (Fig. 1D). This reduction in tumor growth translated to a significant albeit modest increase in survival in the AKTi + Gem cohort (Supplementary Fig. S1D and S1E). The reduction in tumor growth upon combination therapy of MEKi and AKTi translated into a modest prolongation of the survival when compared with the vehicle control or Gem monotherapy (median survival = 21 vs. 11 days, MEKi + AKTi and Gem, respectively; $P = 0.037$; Fig. 1E; Supplementary Fig. S1D and S1E). Tumor regressions were elicited upon triple combination treatment with MEKi, AKTi, and Gem, but these were short lived and all mice eventually relapsed and succumbed to their disease (median survival = 34 days, $P < 0.001$ relative to Gem monotherapy; Fig. 1E; Supplementary Fig. S1D and S1E), which is consistent with data from others (31). Together, the short- and long-term treatment of KPC mice mirrors the transient response with limited efficacy at disease control, modeling the resistance that ultimately develops to this treatment regimen in patients.

We explored whether the limited and transient response to the triple combination therapy was due to delivery and/or metabolism of Gem. Although other therapies, such as Hedgehog pathway inhibitors, have been shown to alter delivery of therapies to PDA tumors (26), we observed no differences in intratumoral concentration of Gem and its metabolites, indicating the observed effect in mice was not due to alterations in Gem delivery or metabolism (Supplementary Fig. S1F). In addition, activation of several RTKs, including EGFR, ERBB2, ERBB3, IGF-1R, INS-R, and MET, has been previously implicated in the acquisition of resistance to single-agent targeting of MEK or AKT (16–20). Based on this data, we set to investigate whether the activation of RTKs occurs upon dual MEK and AKT blockade *in vivo*. For this purpose, we evaluated the phosphorylation status of 39 RTKs (Fig. 1F; Supplementary Fig. S2A). Dual blockade of MEK and AKT had inconsistent effects on Egfr phosphorylation, but induced elevations of ErbB2 phosphorylation, relative to vehicle control (Supplementary Fig. S2A).

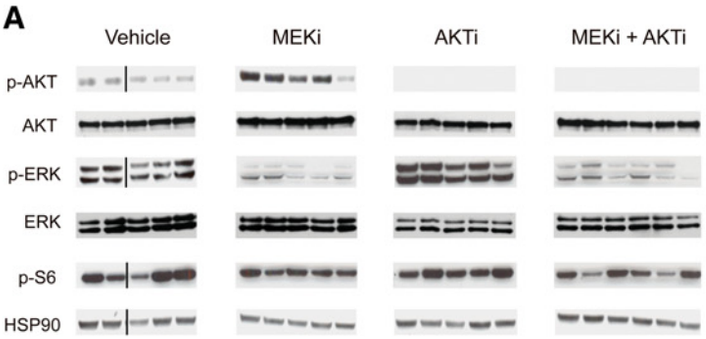

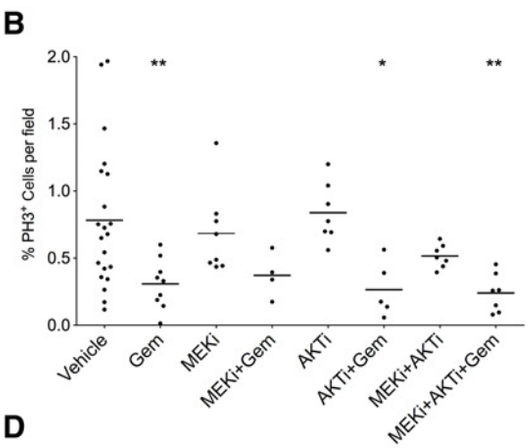

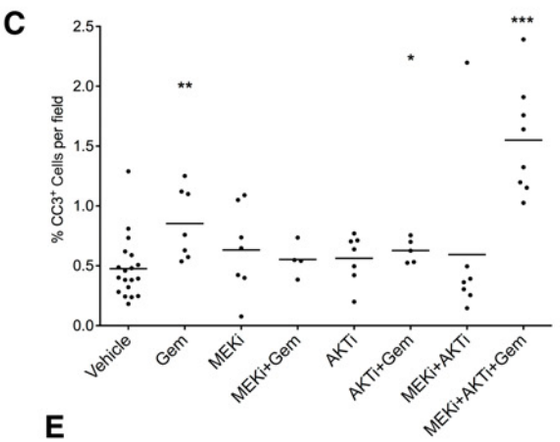

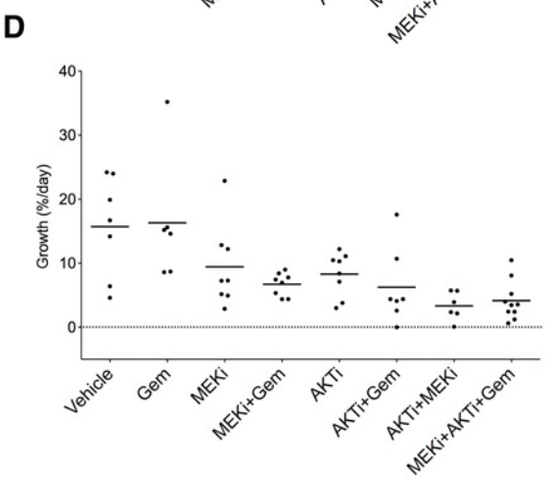

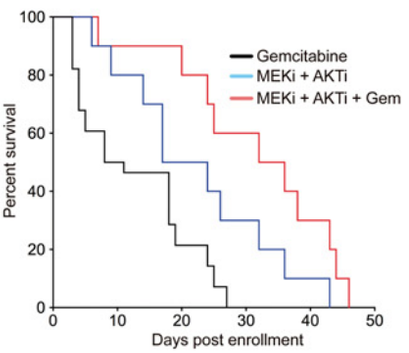

Treatment	*N*	Median survival	*P*
Gemcitabine	17	11	N/A
AKTi + MEKi	10	21	0.037
AKTi + MEKi + Gemcitabine	10	34	<0.001

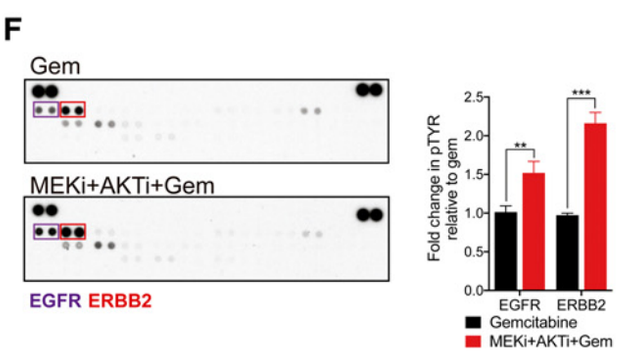

The triple combination of Gem, MEKi, and AKTi also elicited elevation of Egfr and ErbB2 phosphorylation relative to Gem monotherapy ($n = 3/3$), whereas other RTK phosphorylation changes were inconsistent (Fig. 1F).

Taken together, our results show that the combination of MEK and AKT pathways has a modest effect on survival in mice, and that the activation of ErbB signaling occurs in mouse PDA in response to inhibition of the MEK and AKT pathways.

ERBB family signaling is activated as a malignant-specific resistant mechanism in response to MEK and AKT inhibition

To study the biochemical adaptive changes in normal or malignant contexts, we determined the efficacy of MEKi and AKTi in murine organoid cultures (22). Organoids were generated from healthy, nontransformed epithelial cells of mouse normal pancreata (mN, $n = 3$), and pancreatic tumors (mT) from the KPC model ($n = 3$). Following treatment with AKTi and MEKi for 72 hours as single agents, mT were more resistant than mN organoids (Fig. 2A and B; Table 1). Although mT organoids were generally more resistant to single-agent treatments, the combination of MEKi and AKTi had similar efficacy in both mT and mN cultures (Fig. 2C and Table 1).

Short-term (2 hours) AKTi or MEKi treatment inhibited phosphorylation of their respective targets in both mT and mN organoids (Fig. 2D and E). Robust inhibition of S6 phosphorylation was reached only when both AKT and MEK were inhibited (Fig. 2D). Reactivation of AKT and ERK was observed after 60 hours of dual MEK and AKT blockade in mT organoids (Fig. 2D). On the other hand, both pathways remained inactivated in mN organoids (Fig. 2E). These data show that target inhibition is maintained in the normal organoids, but lost in the malignant context.

Next, we sought to identify RTK gene expression changes in response to MEK and AKT blockade in organoids. For this purpose, the relative abundance of mRNA encoding selected RTKs (*Egfr*, *ErbB2*, *ErbB3*, *Igf-1r*, *Ins-r*, and *Met)* was measured by qRT-PCR following single- or dual-agent treatment for 72 hours. Expression of *Egfr* mRNA was significantly induced in mT but not mN organoids following single- and dual-agent treatments for 72 hours relative to the vehicle controls (Fig. 2F). The gene expression levels of other RTKs were not consistently affected by any of the treatments.

To evaluate the activation status of RTKs, we measured their total and phosphorylated levels in mN and mT organoids following MEK and AKT inhibition. The combination of MEKi and AKTi resulted in elevation of both total and phosphorylated Egfr in mT organoids (Fig. 2G and H). mN organoids similarly elevate total levels of Egfr, but without increased phosphorylation (Fig. 2G and H). Phosphorylation of ErbB2 was not elevated in mT organoids following single- or dual-agent treatment. Comprehensive evaluation of the phosphorylation status of other RTKs confirmed the elevation in phosphorylated Egfr in mT organoids following dual MEK and AKT inhibition relative to vehicle controls, but no other changes in RTK activation status (Fig. 2I; Supplementary Fig. S2B). Overall, these data demonstrate that the concomitant inhibition of MEK and AKT results in activation of ErbB family members in mouse pancreatic tumor–derived organoid cultures, but not their normal counterparts.

To assess whether these biochemical adaptive mechanisms translate to human PDA, we determined the *in vitro* cytotoxicity of MEKi and AKTi in human pancreatic ductal organoids (22). Human PDA organoid cultures [$KRAS^{G12V}$-mutant human tumor (hT) organoids, $n = 2$ and $KRAS^{G12D}$-mutant human metastatic (hM) organoid culture, $n = 1$] and human normal (hN) organoid cultures ($KRAS^{wt}$, $n = 3$) were used for this study. All of these organoids responded similarly to MEKi or AKTi treatment as single agents or in combination (Fig. 3A–C and Table 1). MEKi and AKTi monotherapies inhibited MAPK and PI3K signaling, respectively, in organoid cultures within 2 hours (Fig. 3D).

RTK mRNA levels were evaluated in organoids after treatment with MEKi, AKTi, and a combination of both for 72 hours. The mRNA levels of *ERBB2*, *ERBB3*, *IGF-1R*, and *INS-R* were highly elevated in hT/hM organoids treated with the MEKi/AKTi combination for 72 hours, relative to vehicle control, whereas levels of *EGFR* were not consistently changed (Fig. 3E; Supplementary Fig. S2C). Following combined treatment with MEKi and AKTi, mRNA expression of *ERBB2* and *ERBB3* in hN organoids was unchanged or modestly increased relative to vehicle (Fig. 3F; Supplementary Fig. S2C). Larger changes were observed in *IGF-1R* and *INS-R* in hN organoids following dual MEK and AKT inhibition, whereas *EGFR* and *MET* levels did not consistently change in response to treatment in hN and hT/hM organoids (Fig. 3E and F; Supplementary Fig. S2C). Single-agent administration of MEKi did not increase the transcript levels of most RTKs in hT/hM organoids, which is in contrast to prior reports using monolayer cultures of *KRAS*-mutant colorectal and non–small cell lung cancer (17–19).

We sought to explore whether the same resistance mechanisms persist after conversion of the organoids into monolayer cultures. Upon conversion of the hM1 organoid line into a monolayer culture (hM1-2D), we found robust elevation in the mRNA levels of *EGFR*, *ERBB2*, *ERBB3*, *IGF-1R*, *INS-R*, and *MET* in all treatment regimens (Supplementary Fig. S2D). Similar results were obtained after treatment of established human PDA cell lines with MEKi and AKTi treatment (Supplementary Fig. S2D). These data suggest that the induction of RTK gene expression by MEKi and AKTi may be dependent on the dimensional context in which it is evaluated.

Figure 1.

Analysis of the efficacy of combined treatment with MEK and AKT inhibitors in a mouse model of pancreatic cancer. **A,** *Kras*$^{+/LSL\text{-}G12D}$; *Trp53*$^{+/LSL\text{-}R172H}$; *Pdx1-Cre* (KPC) mice were treated for 7 days with vehicle, MEKi, AKTi, or a combination of MEKi and AKTi. Five tumors per group were analyzed by immunoblot for activation of the respective signaling pathways. Hsp90 was used as a loading control. The line separates different blots. **B,** Percentage of proliferating cells within the tumor mass was measured by staining tissue sections from KPC-treated mice for phospho-histone H3 (PH3). Lines indicate mean percentage values. *, $P < 0.05$; **, $P < 0.01$; and ***, $P < 0.001$ relative to vehicle control by one-way ANOVA with Dunnett multiple comparison test and single pooled variance. **C,** Percentage of apoptotic cells for cleaved caspase (CC3), presented as in **B**. **D,** Percentage of tumor growth (shown as percentage per day) for the different treatment groups. Lines indicate mean growth values. *, $P < 0.05$; **, $P < 0.01$; and ***, $P < 0.001$ relative to vehicle control by one-way ANOVA with Dunnett multiple comparison test and single pooled variance. **E,** Survival curves of KPC mice treated with vehicle, gemcitabine, MEKi + AKTi, or with MEKi + AKTi + gemcitabine. **F,** Quantification of changes in phosphorylation of Egfr and ErbB2 detected by phospho-RTK array is displayed on the right, with error bars indicating SD of the mean.

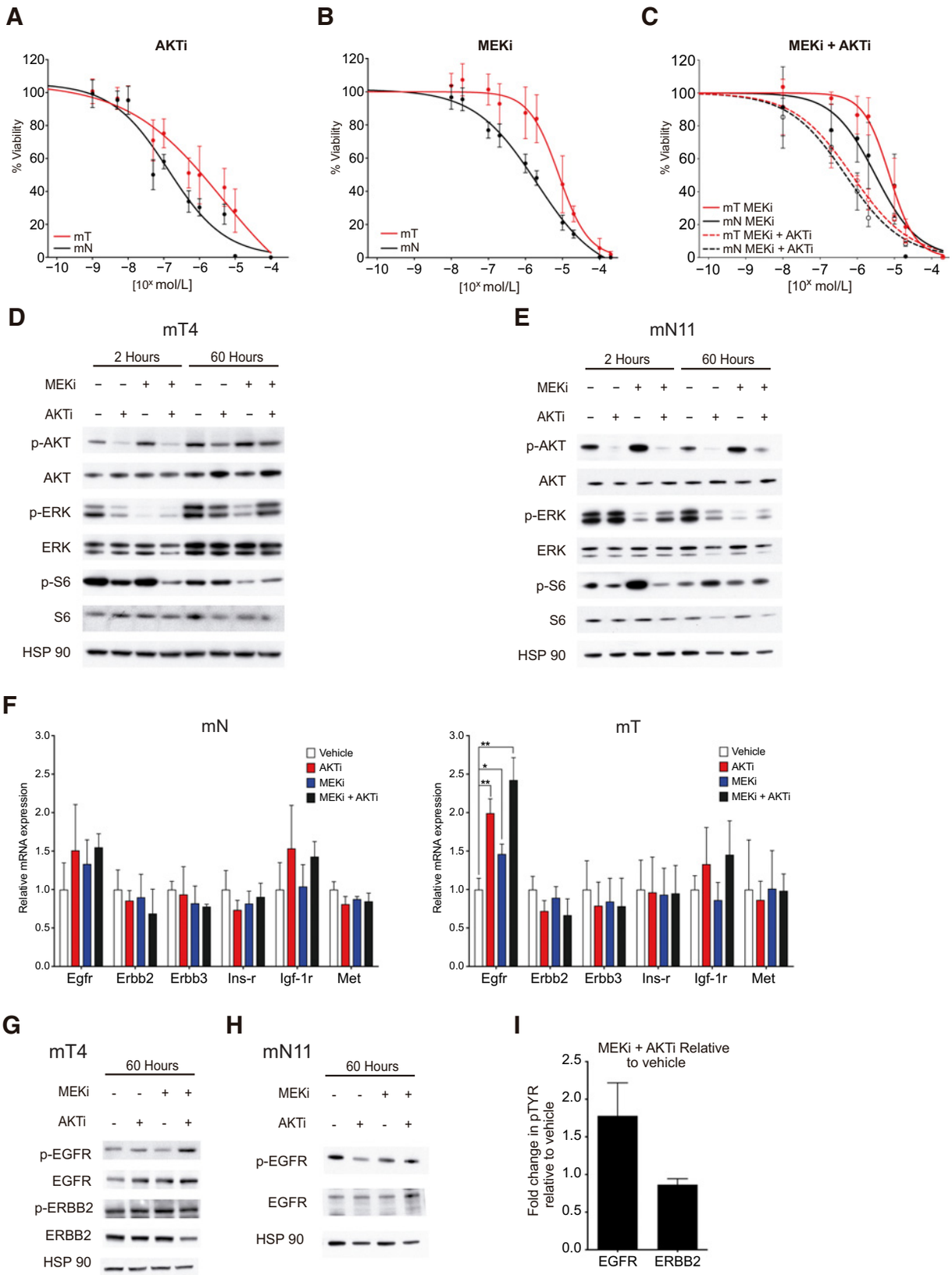

To broadly evaluate RTK activation following MEK and AKT blockade, we quantified the fold change in phospho-RTK arrays following 48 hours of treatment in hN and hT/hM cultures. We observed an increase in the phosphorylation of ERBB2, IGF-1R, and INS-R in two out of the three hT/hM cultures and ERBB3 in a single hT/hM culture (Fig. 3G and H; Supplementary Fig. S2E). In contrast, when evaluated in a monolayer context (hM1-2D), their response to dual MEK and AKT inhibition primarily resulted in the hyperphosphorylation of EGFR and ERBB2 (Supplementary Fig. S2G). When hN organoids were subjected to the same treatment, we detected an increase in phosphorylated IGF-1R and INS-R, but phosphorylation of ERBB family members was either unchanged or undetectable (Fig. 3G and H; Supplementary Fig. S2F).

We then confirmed the activation of ERBB receptors in hT/hM organoids using Western blot analyses. Single and/or dual MEKi and AKTi administration for 72 hours increased total and phosphorylated ERBB2 and ERBB3 in hT/hM organoids, whereas EGFR phosphorylation was unchanged (Figs. 3I and 4H; Supplementary Fig. S2H).

Different ERBB family members are activated in the mouse and human monolayer culture, organoid, and mouse model systems. Regardless, the pathway as a whole was consistently hyperactivated in response to dual MEK and AKT blockade. On the other hand, activation of INS-R and IGF-1R occurs regardless of neoplastic status following dual blockade of MEK and AKT. Taken together, the tumor-specific, universal, and overall activation of ERBB signaling as a resistance mechanism to MEK and AKT inhibition across all models nominates this pathway as a therapeutic target.

Table 1. EC_{50} of mouse and human organoids treated with the indicated antagonists; individual experiments are separated by a thick line; EC_{50} is shown as the average and the 95% CI in parenthesis

Drug(s)	hT	hN	mT	mN
MEKi	11 μmol/L (7–15)	12 μmol/L (9–14)	8 μmol/L (6.8–9.1)	2 μmol/L (1.6–5.3)
AKTi	12 μmol/L (10–14)	70 μmol/L (50–90)	4.3 μmol/L (0.8–8)	0.14 μmol/L (0.1–0.2)
MEKi + AKTi	3 μmol/L (2.1–4.5)	3.9 μmol/L (2.3–5.5)	0.7 μmol/L (0.5–1)	0.5 μmol/L (0.3–0.8)
MEKi + AKTi + ERBBi	0.4 μmol/L (0.3–0.5)		0.1 μmol/L (0.07–0.15)	
MEKi + ERBBi	0.5 μmol/L (0.4–0.7)			
ERBBi	1.5 μmol/L (0.9–2.3)		1.2 μmol/L (0.7–1.7)	
ERBBi	1.3 μmol/L (1–2)		1.2 μmol/L (0.8–1.6)	
EGFRi	12 μmol/L (10–14)		5 μmol/L (3–7)	
AKTi	5.3 μmol/L (2.1–8.4)		3 μmol/L (2–4)	
AKTi + EGFRi	3.2 μmol/L (2–5.3)		0.6 μmol/L (0.5–0.7)	
AKTi + ERBBi	0.8 μmol/L (0.6–1.3)		0.5 μmol/L (0.4–0.6)	
MEKi	6.5 μmol/L (4.5–7.3)		6 μmol/L (5.5–7.7)	
MEKi + EGFRi	3.6 μmol/L (3.2–4.2)		0.6 μmol/L (0.5–0.7)	
MEKi + ERBBi	0.6 μmol/L (0.5–0.8)		0.3 μmol/L (0.2–0.3)	

ERBB blockade increases the sensitivity to MEK and AKT inhibition in mouse and human tumor organoids

The human organoid data suggest that heterodimeric complexes involving ERBB2/ERBB3 are putative mediators of resistance to MEK and AKT inhibition in PDA, whereas in mouse organoids the feedback to dual MEK and AKT blockade results in activation of Egfr. Therefore, we compared the *in vitro* efficacy of an irreversible pan-ERBB kinase inhibitor (neratinib, ERBBi) to an EGFR-specific inhibitor (erlotinib, EGFRi). Both mouse and human tumor organoids were more sensitive to ERBBi than EGFRi (Supplementary Fig. S3A; Table 1). However, although both ERBBi and EGFRi sensitized mT organoids to MEKi or AKTi (Fig. 4A–C and Table 1), ERBBi was more efficient than EGFRi in sensitizing hT/hM cultures to either MEK or AKT inhibition (Fig. 4D–F and Table 1).

ERBBi also significantly increased the sensitivity of both mouse and human PDA organoids to the combination of MEKi and AKTi (Fig. 4C and F). Pan-ERBB inhibition prevented hyperphosphorylation of EGFR in mT organoids and elevated phosphorylation of ERBB2 and ERBB3 in hT/hM organoids following MEKi and AKTi treatment (Fig. 4G and H). The reacquisition of ERK, AKT, and S6 phosphorylation induced by prolonged MEKi and AKTi treatment was averted by addition of ERBB inhibition in both mouse and human tumor organoids despite elevation of total protein levels (Fig. 4G and H).

Treatment with both MEK and AKT inhibitors has been reported to exhibit severe and common dose-limiting toxicities in the clinic (13, 32). Therefore, we assessed the tolerability of the triple combination of MEKi, AKTi, and ERBBi in C57Bl/6J mice with two different dose levels ($n = 3$ for each dose level). Treatment with all three inhibitors led to severe adverse reactions and all mice succumbed within 4 to 7 days of treatment (data not shown), discouraging further exploration of this therapeutic strategy *in vivo*.

To avert the extreme toxicities associated with combined inhibition of MEK, AKT, and ERBB signaling, we evaluated the efficacy of alternative combinations. Synergy studies are more amenable in culture than *in vivo*. Therefore, we chose to further investigate the efficacy of the alternative combinations in organoids before proceeding to mouse studies. As an alternative to the combination

Figure 2.

MEK and AKT inhibition promotes Egfr expression and phosphorylation in murine pancreatic organoids. **A–C,** Dose–response curves of mN and mT organoids treated with AKTi alone (**A**), MEKi alone (**B**), and MEKi or a combination of both AKTi and MEKi (**C**). $n = 3$ for each group. Error bars indicate SD. **D** and **E,** Immunoblot analysis of MEK and AKT pathway status in mT organoids (**D**) and mN organoids (**E**) treated for 2 or 60 hours with single or combination therapies. Hsp90 is shown as a loading control. **F,** Changes in mRNA levels of ErbB receptors and other RTKs measured by qRT-PCR in mN and mT organoids, following treatment for 72 hours with single and dual inhibition of MEK and AKT. $n = 3$ per group (*, $P < 0.05$; **, $P < 0.01$; and ***, $P < 0.001$). **G** and **H,** Immunoblot analysis of ErbB pathway activation status in mT organoids (**G**), and Egfr activation status in mN organoids (**H**) treated for 60 hours with single or combination therapies. Hsp90 is shown as a loading control. Hsp90 is shown as a loading control. **I,** Quantification of phospho-RTK array for mT organoids treated for 48 hours with either DMSO (vehicle) or MEKi and AKTi. Changes in phospho-RTK levels are quantified, and error bars indicate SD of the mean.

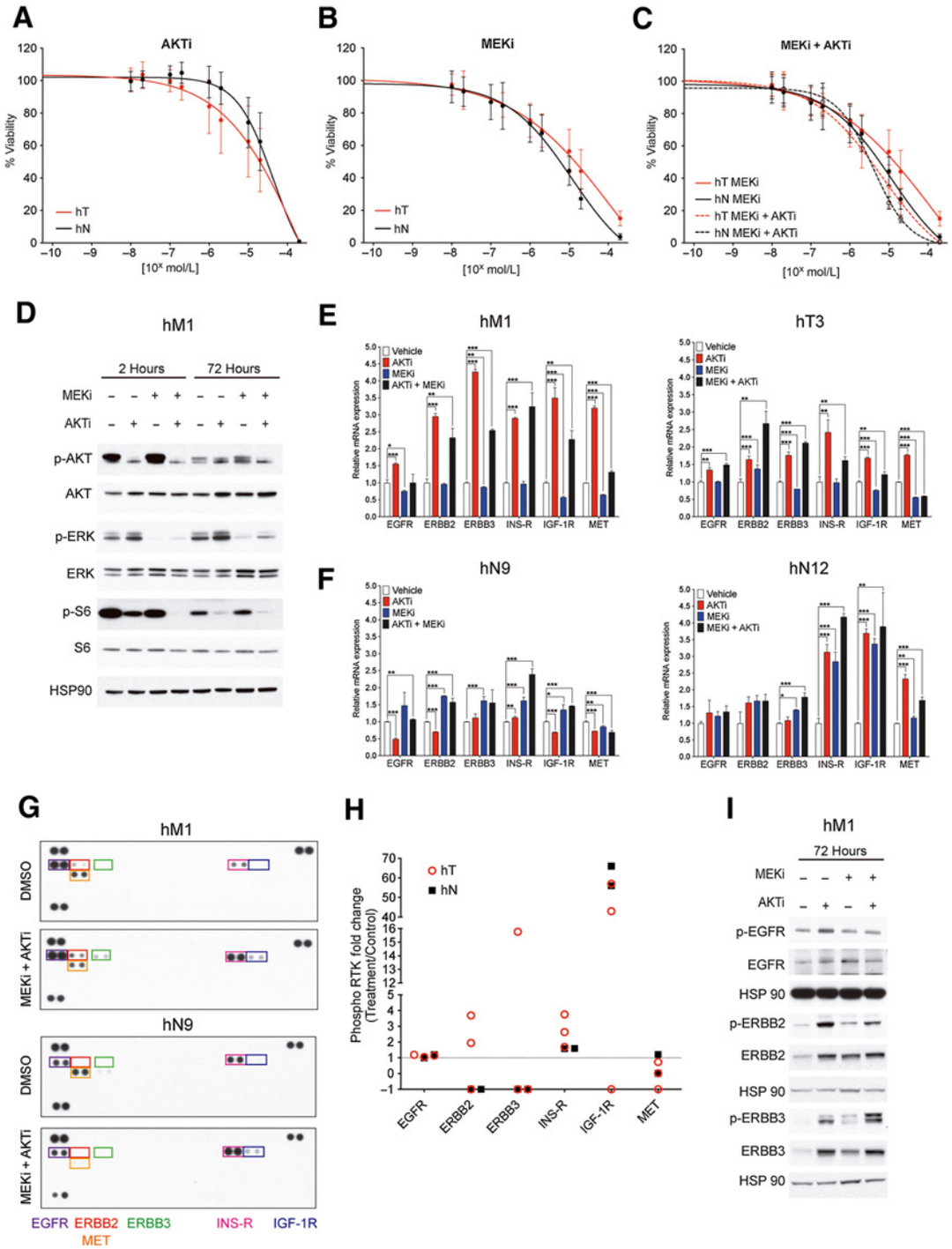

Figure 3.

Combined inhibition of MEK and AKT promotes ERBB2/3 expression and phosphorylation in human pancreatic organoids. **A–C,** Dose–response curves of human T organoids (hT) and human normal organoids (hN) treated with AKTi (**A**) and MEKi (**B**), and MEKi + AKTi (**C**). $n = 3$ per each group. **D,** Immunoblot analysis of MEK and AKT pathway activation status in hM1 organoids treated for 2 or 72 hours with single or combination therapies. Hsp90 is shown as a loading control. **E** and **F,** Changes in mRNA levels of ERBB family members and other RTKs in hT organoids (**E**) and hN organoids (**F**) following 72-hour treatment with MEK and AKT inhibitors as single agents or in combination. $n = 3$ per group (*, $P < 0.05$; **, $P < 0.01$; and ***, $P < 0.001$). **G,** Representative phospho-RTK arrays for human tumor and normal organoids. **H,** Quantification of changes in phospho-RTK levels after treatment with the combination of MEKi and AKTi for 48 hours relative to DMSO controls. Values less than 0 indicate nondetectable signal. **I,** Immunoblot analysis of ERBB pathway activation status hM1 organoids treated for 72 hours with single or combination therapies. Hsp90 is shown as a loading control.

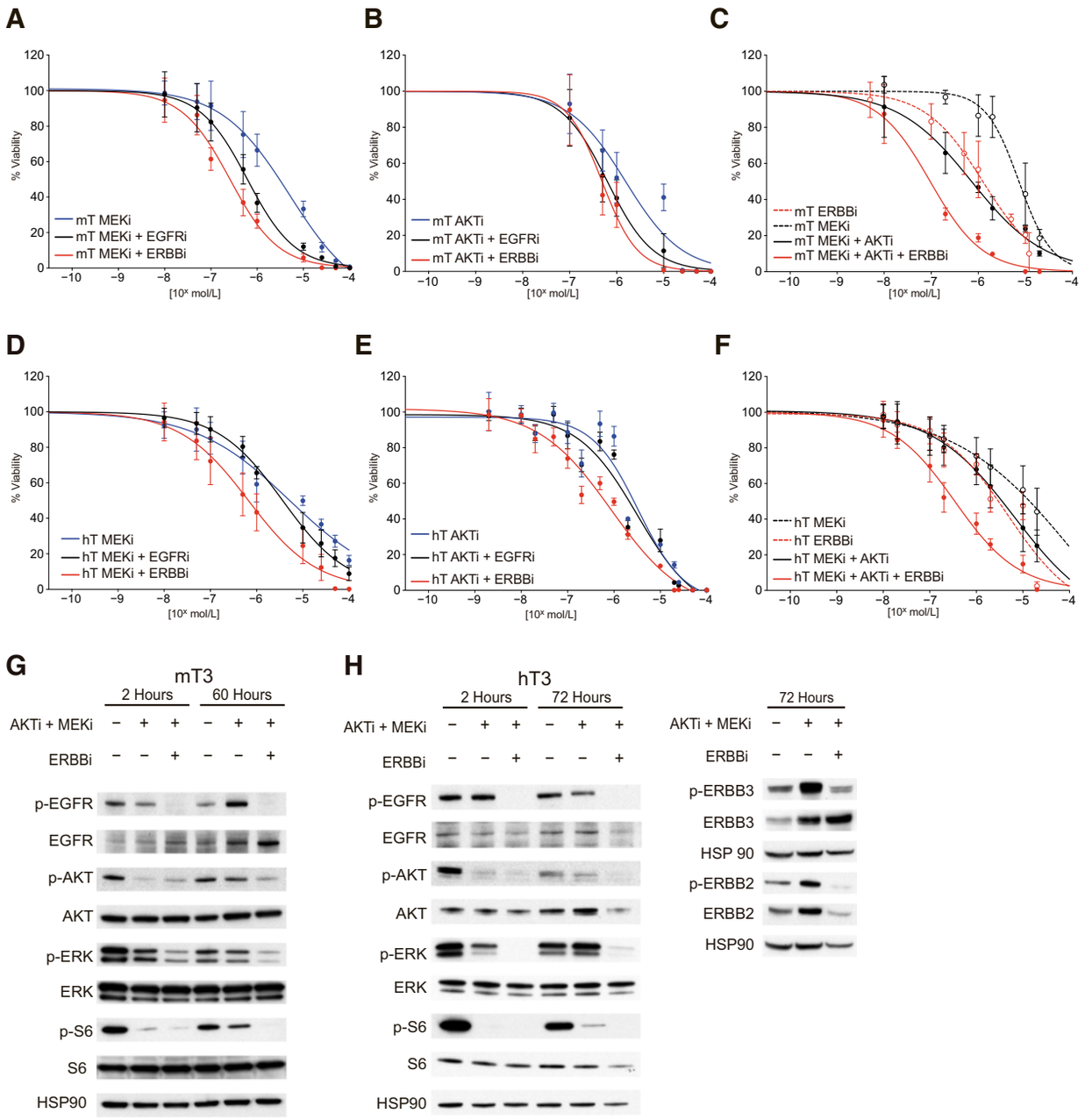

Figure 4.

Pan-ERBB kinase inhibition is more effective than EGFR inhibition alone in human tumor organoids. **A–C**, Dose–response curves of mT organoids ($n = 3$) treated with MEKi, MEKi + EGFRi, or MEKi + ERBBi (**A**); AKTi, AKTi + EGFRi, or AKTi + ERBBi (**B**); MEKi, ERBBi, MEKi + AKTi; or MEKi + AKTi + ERBBi (**C**). For all dose–response curves, error bars represent SD. **D–F,** Dose–response curves of hT organoids ($n = 3$) treated with MEKi, MEKi + EGFRi, or MEKi + ERBBi (**D**); AKTi, AKTi + EGFRi, or AKTi + ERBBi (**E**); and MEKi, ERBBi, MEKi + AKTi, or MEKi + AKTi + ERBBi (**F**). For all dose–response curves, error bars represent SD. **G,** Immunoblot analysis of mT3 organoids treated for 2 or 60 hours with MEKi + AKTi or MEKi + AKTi + ERBBi. Hsp90 is shown as a loading control. **H,** Immunoblot analysis of hT3 organoids treated for 2 or 72 hours with MEKi + AKTi or MEKi + AKTi + ERBBi.

of all three inhibitors, we examined the efficacy of ERBBi in combination with single-agent MEKi or AKTi relative to the combination of all three antagonists. Although combination of ERBBi and AKTi was not as effective as the triple combination, dual administration of ERBBi with MEKi was sufficient to achieve maximal levels of cytotoxicity (Fig. 5A–C and Table 1). We then determined whether EGFRi and ERBBi were synergistic with either MEKi or AKTi by measuring the CI (25). The CI value represents the synergistic effect of drug combinations, with CIs of <1, 1, and >1 indicating synergism, additive effects, and antagonism, respectively. The combination of ERBBi with MEKi or AKTi was synergistic in two different human PDA-derived organoids

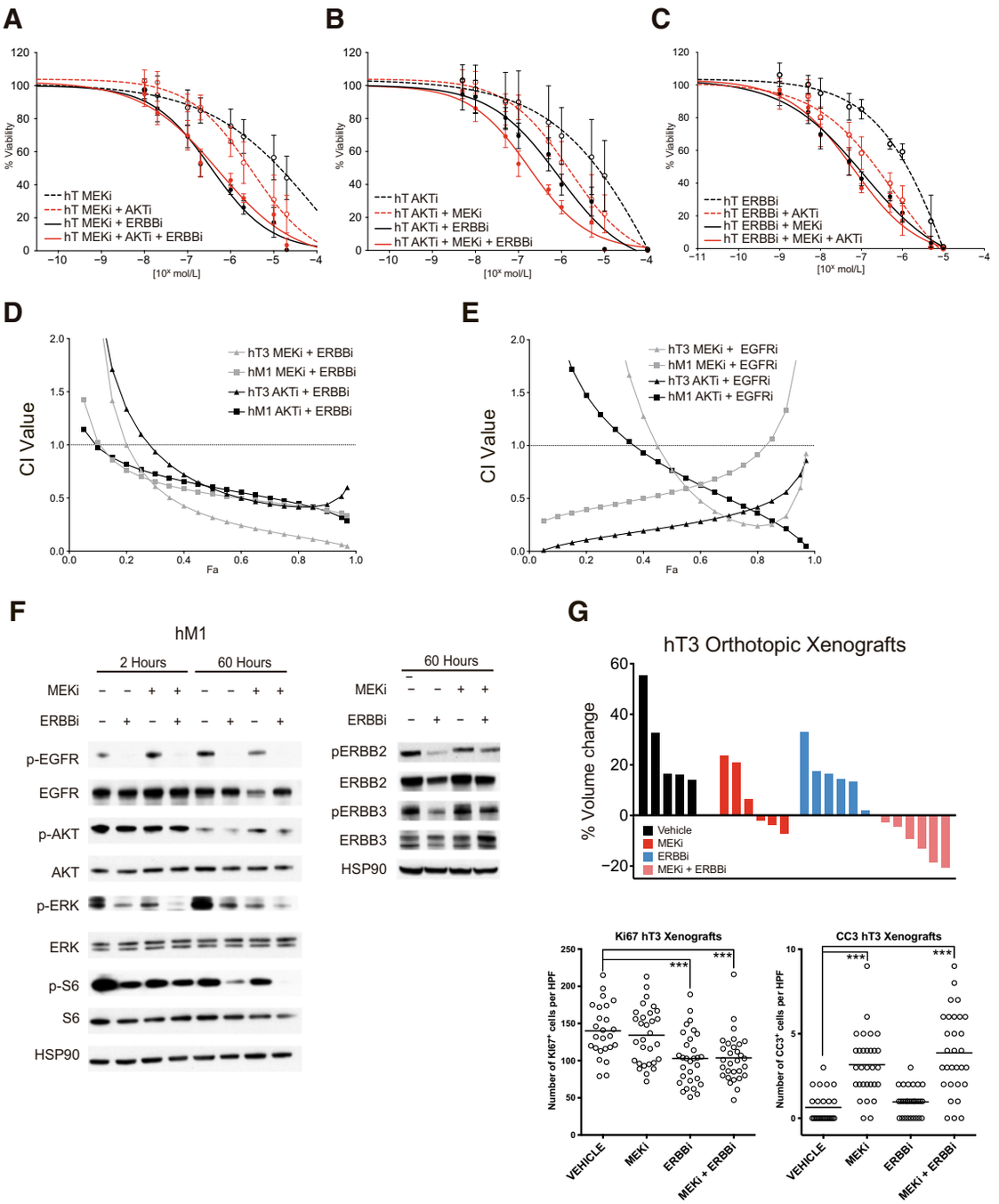

Figure 5.

Combination of Pan-ERBB kinase and MEK inhibitors achieves similar efficacy to the triple combination. **A–C**, Dose–response curves of hT ($n = 3$) organoids treated with MEKi, MEKi + AKTi, MEKi + ERBBi, or MEKi + AKTi + ERBBi (**A**); AKTi, AKTi + MEKi, AKTi + ERBBi, AKTi + MEKi + ERBBi (**B**); ERBBi, ERBBi + AKTi, ERBBi + MEKi, or MEKi + AKTi + ERBBi (**C**). For all dose–response curves, error bars represent SD. **D** and **E,** CI plots for the dual combinations of MEKi + ERBBi and AKTi + ERBBi (**D**) and AKTi + EGFRi and MEKi + EGFRi (**E**) in two human PDA organoids. CI values were plotted as a function of fractional inhibition for the fraction affected (Fa) range of 0.10 to 0.97. **F,** Immunoblot analysis of hM1 organoids treated for 2 or 60 hours with ERBBi, MEKi, or ERBBi + MEKi. Hsp90 is shown as a loading control. **G,** Waterfall plot of individual tumor volume changes as measured by ultrasound using human tumor xenografts *in vivo* treated with Pan-ERBB kinase and MEK inhibitors (top). Number of proliferating cells within the tumor mass was measured by staining tissue sections from treated mice for Ki67 (bottom left plot). Lines indicate mean. Number of apoptotic cells within the tumor mass was measured by staining tissue sections from treated mice for cleaved caspase (CC3; bottom right plot). *, $P < 0.05$; **, $P < 0.01$; ***, $P < 0.001$; and ****, $P < 0.0001$ relative to vehicle control by two-tailed Mann–Whitney nonparametric *t* test.

Table 2. CI of drug combinations in human tumor and metastatic (hT and hM) organoids

CI at:	Fa50	Fa90	Fa95	Fa97
AKTi + EGFRi				
hM1	0.96	0.40	0.30	0.25
hT3	0.43	0.75	0.92	1.06
MEKi + EGFRi				
hM1	0.75	1.53	2.21	2.98
hT3	0.97	0.53	0.80	1.15
AKTi + ERBBi				
hM1	0.60	0.37	0.32	0.28
hT3	0.59	0.43	0.52	0.59
MEKi + ERBBi				
hM1	0.54	0.38	0.35	0.33
hT3	0.31	0.09	0.06	0.04

(hM1 and hT3) at high levels of fraction affected (Fig. 5D and E; Table 2). Treatment with the combination of EGFRi with AKTi or MEKi was inconsistent and antagonistic, respectively. Following long-term (60 hours) exposure to combined MEKi and ERBBi treatment, the phosphorylation of EGFR, ERK, and S6 remained inhibited, indicating successful and sustained attenuation of pathway (Fig. 5F). Altogether, these data suggest that synergy between MEK and pan-ERBB pathway inhibition will be efficacious *in vivo*.

Given the synergy between MEK and pan-ERBB pathway inhibition in human cells, we evaluated the efficacy of the ERBBi and MEKi combination therapy in orthotopic xenografts of human tumor organoids. Following orthotopic transplantation of hT3 organoids into NSG mice, the resulting tumors were then passaged once to generate sufficient animals for a short-term intervention study. This transplantation model recapitulates the histology of the primary tumor used to generate the organoid cultures (Supplementary Fig. S3B). Mice were enrolled in a 7-day trial once their tumor reached a minimum volume of 350 mm^3 (Supplementary Fig. S3C and S3D). No significant change in tumor growth was observed upon treatment with single-agent ERBBi or MEKi (Fig. 5G; Supplementary Fig. S3E). In contrast, inhibition of both MEK and ERBB resulted in robust regressions in all mice measured (Fig. 5G; Supplementary Fig. S3E). Although we found that the ERBBi reduced cell proliferation by Ki67 IHC, the MEKi did not have any significant impact on the number of Ki67-positive cells (Fig. 5G; Supplementary Fig. S3F). In contrast, the ERBBi had no effect on cell death, but the MEKi significantly increased the number of cells positive for CC3 by IHC (Fig. 5G; Supplementary Fig. S3G). Importantly, this model predicts that the therapeutic combination of MEK and pan-ERBB inhibition may be clinically useful.

Discussion

In this study, we investigated the potential of a recently developed three-dimensional organoid culture system to serve as a platform for the identification of effective therapeutic strategies in PDA (22). To identify strategies to avert acquisition of resistance without causing excessive adverse side effects, we focused on the evaluation of tumor-specific resistance pathways to combined MEK and AKT inhibition.

EGFR/ERBB and IGF-1R have been identified as resistance mechanisms to dual MEK and AKT blockade and are considered therapeutic targets for PDA (19, 33, 34). Using mouse models and the pancreatic organoid culture system, we identified a similar response to this treatment strategy. However, it was previously unclear whether the ability to evade MEK and/or AKT inhibition was a unique property of cancer cells because of the inability to propagate normal, nontransformed pancreatic epithelial cells in the same media conditions. The organoid system enables culture of both normal nontransformed cells and malignant cells in the same media. With this comparator, we were able to determine that elevation of IGF-1R and INS-R phosphorylation in response to MEK and AKT inhibition is common to both normal and malignant cells. Therefore, targeting these pathways may result in deleterious and dose-limiting side effects. Although we found that both two-dimensional culture and organoid models identified ERBB signaling as a resistance mechanism, we were able to distinguish common cellular responses observed in both normal and tumor cells versus a resistance mechanism unique to the malignant state only using the organoid model. This advantage enabled us to prioritize targeting the ERBB signaling pathway as it was not activated in normal organoids following MEK and AKT inhibition rather than the INS-R and IGFR signaling pathways that were activated in both normal and malignant organoids.

In line with this, EGFR and ERBB2 are activated *in vivo* following therapeutic challenge with MEKi and AKTi in tumor-bearing KPC mice. Combination of a pan-ERBB kinase inhibitor with an MEK antagonist was synergistic in human tumor organoids and resulted in a robust increase in cytotoxicity. Therefore, we evaluated the therapeutic combination of MEKi and ERBBi in xenografts of human tumor organoids. Previously, we established human organoid–based orthotopic xenograft models in which tumors derived from organoids faithfully recapitulate PDA progression and pathophysiologic features of human PDA tissues (22) unlike tumors derived from cell-based and/or subcutaneous xenografts. In order to accelerate our ability to evaluate the efficacy of new combination treatment strategies *in vivo*, we developed a second-generation organoid xenograft model where the organoid-derived tumor pieces were passaged and transplanted into the pancreata of immunocompromised mice. This xenograft model mimics the desmoplasia observed in human PDA and serves as a rapid platform for therapeutic intervention studies. We found that combination of MEKi and ERBBi resulted in robust tumor regression in a second-generation organoid-based xenograft model.

Interestingly, a recent publication described the results of a phase II trial of selumetinib (MEKi) plus erlotinib (EGFRi) in chemotherapy-refractory, advanced PDA (35). The results of the trial showed no objective response in any of the 46 treated patients, which is consistent with our *in vitro* findings that EGFRi alone is not sufficient to sensitize human PDA organoids to MEK inhibition. These results suggest that evaluation of these biochemical adaptive changes in different culture models yields a more comprehensive prediction of the pathways utilized in acquisition of resistance to targeted agents. In addition, a new allosteric AKT inhibitor in combination with the Erk inhibitor, trametinib, has shown 1 durable partial response out of 3 patient-derived xenografts of KRAS-mutant PDA (36). Together, our and others' data from monolayer cultures combined with the data from our organoid and *in vivo* experiments suggest that complete abrogation of ERBB signaling is required to circumvent resistance. Along these lines, treatment with an EGFR/ERBB2 inhibitor (lapatinib) that also attenuated ERBB3 phosphorylation in combination with an MEK inhibitor (trametinib) exhibited antitumor

activity relative to monotherapies in PDA xenografts (37). Recently, two independent groups showed that cotreatment with pan-ERBB inhibitors (neratinib and/or afatinib) and MEK inhibitors can impair *Kras*-driven lung tumorigenesis, which is also consistent with our therapeutic studies with MEKi and ERBBi in xenografts of human PDA organoids (38, 39). These results strengthen the conclusion that combination of a pan-ERBB inhibitor with MEK antagonists may improve patient outcome.

Disclosure of Potential Conflicts of Interest

T.E. Bapiro is an employee of and has ownership interests (including patents) at AstraZeneca. P. Huang is an employee of Cygnal Therapeutics, and has ownership interests in Merck, Roche, and GlaxoSmithKline. P. Smith has ownership interests (including patents) at AstraZeneca. K.H. Yu reports receiving speakers bureau honoraria from and is a consultant/advisory board member for Ipsen, reports receiving commercial research grants from Halozyme and Bristol-Myers Squibb, and testified as an expert witness regarding Novartis drug everolimus. D.I. Jodrell reports receiving commercial research grants and commercial research support from AstraZeneca. D.A. Tuveson has ownership interests (including patents) at and is a consultant/advisory board member for Leap Therapeutics and Surface Oncology, and reports receiving commercial research grants from Fibrogen and ONO. No potential conflicts of interest were disclosed by the other authors.

Authors' Contributions

Conception and design: M. Ponz-Sarvise, V. Corbo, H. Tiriac, D.D. Engle, P. Huang, K.H. Yu, Y. Park, D.A. Tuveson

Development of methodology: M. Ponz-Sarvise, V. Corbo, H. Tiriac, D.D. Engle, T.E. Oni, C.-I. Hwang, I.I.C. Chio, L.A. Baker, K.H. Yu, D.A. Tuveson

Acquisition of data (provided animals, acquired and managed patients, provided facilities, etc.): M. Ponz-Sarvise, V. Corbo, H. Tiriac, D.D. Engle, K.K. Frese, T.E. Oni, C.-I. Hwang, D. Öhlund, D. Filippini, K. Wright, T.E. Bapiro, K. H. Yu, D.I. Jodrell, Y. Park

Analysis and interpretation of data (e.g., statistical analysis, biostatistics, computational analysis): M. Ponz-Sarvise, V. Corbo, H. Tiriac, D.D. Engle, K.K. Frese, T.E. Oni, I.I.C. Chio, K. Wright, K.H. Yu, D.I. Jodrell

Writing, review, and/or revision of the manuscript: M. Ponz-Sarvise, V. Corbo, H. Tiriac, D.D. Engle, T.E. Oni, I.I.C. Chio, L.A. Baker, P. Huang, P. Smith, D.I. Jodrell, Y. Park, D.A. Tuveson

Administrative, technical, or material support (i.e., reporting or organizing data, constructing databases): D.D. Engle, D. Öhlund, K. Wright, T.E. Bapiro

Study supervision: M. Ponz-Sarvise, V. Corbo, D.D. Engle, Y. Park, D.A. Tuveson

Acknowledgments

The authors thank Frances Connor, Paul Mackin, and Lisa Young for maintenance and management of mouse colonies, as well as staff from the Cambridge Institute BRU, histology core, and pharmacokinetics core. MK2206 concentrations were measured by Hiroshi Hirai of Merck Research Laboratories. This research was supported by the University of Cambridge and Cancer Research UK, The Li Ka Shing Foundation and Hutchison Whampoa Limited and the NIHR Cambridge Biomedical Research Centre. K.K. Frese was supported under the NIH Ruth L. Kirschstein National Research Service Award F32CA123887-01, and K.K. Frese and D.A. Tuveson were supported by the European Community Grant EPC-TM-Net 256974. T.E. Bapiro was supported by Cancer Research UK. D.I. Jodrell is a Group Leader in the Cancer Research UK Cambridge Research Institute.

D.A. Tuveson is a distinguished scholar of the Lustgarten Foundation and Director of the Lustgarten Foundation-designated Laboratory of Pancreatic Cancer Research. This work was performed with assistance from the Animal, Microscopy, Animal and Tissue Imaging, and DNA Sequencing CSHL Cancer Center Shared Resources, which are supported by the Cancer Center Support Grant 5P30CA045508. D.A. Tuveson is also supported by the Cold Spring Harbor Laboratory Association, and the PMRA. This research was also supported by a Stand Up To Cancer Phillip A. Sharp Innovation in Collaboration Award, Grant Number SU2C-AACR-PS09 (to D.A. Tuveson). Stand Up to Cancer is a division of the Entertainment Industry Foundation, administered by the American Association for Cancer Research. In addition, the authors are grateful for support from the following: the Cold Spring Harbor Laboratory and Northwell Affiliation (Project Lazarus for D.A. Tuveson), the STARR foundation (I7-A718 for D.A. Tuveson), DOD (W81XWH-13-PRCRP-IA for D.A. Tuveson), the Associazione Italiana Ricerca sul Cancro (AIRC-18718, for V. Corbo), Sociedad Española de Oncología Médica (SEOM for M. Ponz-Sarvise), the Swedish Research Council (537-2013-7277 for D. Öhlund), The Kempe Foundations (JCK-1301 for D. Öhlund), the Swedish Society of Medicine (SLS-326921 and SLS-250831 for D. Öhlund), the Damon Runyon Cancer Research Foundation (DRG-2165-13 for I.I.C. Chio), and the NIH (5P30CA45508-26, 5P50CA101955-07, 1U10CA180944-01, 5U01CA168409-3, 1R01CA190092-01, and 1R01CA188134-01A1 for D.A. Tuveson; R50CA211506 for Y. Park; F32CA180717 for C.-I. Hwang; 5T32CA148056 for L.A. Baker and D.D. Engle; 1K99CA204725-01A1 for D.D. Engle; and P50CA101955 UAB/UMN SPORE for L.A. Baker).

The costs of publication of this article were defrayed in part by the payment of page charges. This article must therefore be hereby marked *advertisement* in accordance with 18 U.S.C. Section 1734 solely to indicate this fact.

Received April 29, 2019; revised June 25, 2019; accepted August 9, 2019; published first September 6, 2019.

References

1. Siegel RL, Miller KD, Jemal A. Cancer statistics, 2018. Ca Cancer J Clin 2018; 68:7–30.
2. Ryan DP, Hong TS, Bardeesy N. Pancreatic adenocarcinoma. N Engl J Med 2014;371:1039–49.
3. Biankin AV, Waddell N, Kassahn KS, Gingras MC, Muthuswamy LB, Johns AL, et al. Pancreatic cancer genomes reveal aberrations in axon guidance pathway genes. Nature 2012;491:399–405.
4. Pylayeva-Gupta Y, Grabocka E, Bar-Sagi D. Ras oncogenes: weaving a tumorigenic web. Nat Rev Cancer 2011;11:761–74.
5. Guerra C, Schuhmacher AJ, Cañamero M, Grippo PJ, Verdaguer L, Pérez-Gallego L, et al. Chronic pancreatitis is essential for induction of pancreatic ductal adenocarcinoma by K-Ras oncogenes in adult mice. Cancer Cell 2007;11:291–302.
6. Hingorani SR, Petricoin EF, Maitra A, Rajapakse V, King C, Jacobetz MA, et al. Preinvasive and invasive ductal pancreatic cancer and its early detection in the mouse. Cancer Cell 2003;4:437–50.
7. Aguirre AJ, Bardeesy N, Sinha M, Lopez L, Tuveson DA, Horner J, et al. Activated Kras and Ink4a/Arf deficiency cooperate to produce metastatic pancreatic ductal adenocarcinoma. Genes Dev 2003;17:3112–26.
8. Fakih M, O'Neil B, Price TJ, Falchook GS, Desai J, Kuo J, et al. Phase 1 study evaluating the safety, tolerability, pharmacokinetics (PK), and efficacy of AMG510, a novel small molecule KrasG12C inhibitor, in advanced solid tumors. J Clin Oncol. 37:15s, 2019 (suppl; abstr 3003).
9. Jones S, Zhang X, Parsons DW, Lin JC, Leary RJ, Angenendt P, et al. Core signaling pathways in human pancreatic cancers revealed by global genomic analyses. Science 2008;321:1801–6.
10. Cox AD, Fesik SW, Kimmelman AC, Luo J, Der CJ. Drugging the undruggable ras: mission possible? Nat Rev Drug Discov 2014;13: 828–51.
11. Alagesan B, Contino G, Guimaraes AR, Corcoran RB, Deshpande V, Wojtkiewicz GR, et al. Combined Mek And Pi3k inhibition in a mouse model of pancreatic cancer. Clin Cancer Res 2015;21:396–404.
12. Junttila MR, Devasthali V, Cheng JH, Castillo J, Metcalfe C, Clermont AC, et al. Modeling targeted inhibition of Mek and Pi3 kinase in human pancreatic cancer. Mol Cancer Ther 2015;14:40–7.
13. Tolcher AW, Khan K, Ong M, Banerji U, Papadimitrakopoulou V, Gandara DR, et al. Antitumor activity in ras-driven tumors by blocking Akt And Mek. Clin Cancer Res 2015;21:739–48.
14. Zhong H, Sanchez C, Spitzer D, Plambeck-Suess S, Gibbs J, Hawkins WG, et al. Synergistic effects of concurrent blockade of Pi3k and Mek pathways in pancreatic cancer preclinical models. Plos One 2013;8: E77243.

15. Chung V, McDonough S, Philip PA, Cardin D, Wang-Gillam A, Hui L, et al. Effect of selumetinib and Mk-2206 vs oxaliplatin and fluorouracil in patients with metastatic pancreatic cancer after prior therapy: swog S1115 study randomized clinical trial. JAMA Oncol 2017;3:516–522.
16. Chandarlapaty S, Sawai A, Scaltriti M, Rodrik-Outmezguine V, Grbovic-Huezo O, Serra V, et al. Akt inhibition relieves feedback suppression of receptor tyrosine kinase expression and activity. Cancer Cell 2011;19: 58–71.
17. Serra V, Scaltriti M, Prudkin L, Eichhorn PJ, Ibrahim YH, Chandarlapaty S, et al. Pi3k inhibition results in enhanced her signaling and acquired Erk dependency in Her2-overexpressing breast cancer. Oncogene 2011;30: 2547–57.
18. Turke AB, Song Y, Costa C, Cook R, Arteaga CL, Asara JM, et al. Mek inhibition leads to Pi3k/Akt activation by relieving a negative feedback on erbb receptors. Cancer Res 2012;72:3228–37.
19. Pettazzoni P, Viale A, Shah P, Carugo A, Ying H, Wang H, et al. Genetic events that limit the efficacy of mek and Rtk inhibitor therapies in a mouse model of kras-driven pancreatic cancer. Cancer Res 2015;75:1091–101.
20. Sun C, Hobor S, Bertotti A, Zecchin D, Huang S, Galimi F, et al. Intrinsic resistance to Mek inhibition in kras mutant lung and colon cancer through transcriptional induction of Erbb3. Cell Rep 2014;7:86–93.
21. Hayes TK, Neel NF, Hu C, Gautam P, Chenard M, Long B, et al. Long-term erk inhibition in kras-mutant pancreatic cancer is associated with myc degradation and senescence-like growth suppression. Cancer Cell 2016;29: 75–89.
22. Boj SF, Hwang CI, Baker LA, Chio II, Engle DD, Corbo V, et al. Organoid models of human and mouse ductal pancreatic cancer. Cell 2015;160: 324–38.
23. Huch M, Bonfanti P, Boj SF, Sato T, Loomans CJ, van de Wetering M, et al. Unlimited in vitro expansion of adult bi-potent pancreas progenitors through the Lgr5/R-spondin axis. Embo J 2013;32:2708–21.
24. Hingorani SR, Wang L, Multani AS, Combs C, Deramaudt TB, Hruban RH, et al. Trp53r172h and Krasg12d cooperate to promote chromosomal instability and widely metastatic pancreatic ductal adenocarcinoma in mice. Cancer Cell 2005;7:469–83.
25. Chou TC. Theoretical basis, experimental design, and computerized simulation of synergism and antagonism in drug combination studies. Pharmacol Rev 2006;58:621–81.
26. Olive KP, Jacobetz MA, Davidson CJ, Gopinathan A, McIntyre D, Honess D, et al. Inhibition of hedgehog signaling enhances delivery of chemotherapy in a mouse model of pancreatic cancer. Science 2009;324:1457–61.
27. Yeh TC, Marsh V, Bernat BA, Ballard J, Colwell H, Evans RJ, et al. Biological characterization of arry-142886 (Azd6244), a potent, highly selective mitogen-activated protein kinase kinase 1/2 inhibitor. Clin Cancer Res 2007;13:1576–83.
28. Li D, Shimamura T, Ji H, Chen L, Haringsma HJ, McNamara K, et al. Bronchial and peripheral murine lung carcinomas induced by T790m-L858r Mutant Egfr Respond To Hki-272 and rapamycin combination therapy. Cancer Cell 2007;12:81–93.
29. Jacobetz MA, Chan DS, Neesse A, Bapiro TE, Cook N, Frese KK, et al. Hyaluronan impairs vascular function and drug delivery in a mouse model of pancreatic cancer. Gut 2013;62:112–20.
30. Bapiro TE, Frese KK, Courtin A, Bramhall JL, Madhu B, Cook N, et al. Gemcitabine diphosphate choline is a major metabolite linked to the kennedy pathway in pancreatic cancer models in vivo. Br J Cancer 2014; 111:318–25.
31. Awasthi N, Kronenberger D, Stefaniak A, Hassan MS, von Holzen U, Schwarz MA, et al. Dual inhibition of the Pi3k and mapk pathways enhances nab-paclitaxel/gemcitabine chemotherapy response in preclinical models of pancreatic cancer. Cancer Lett 2019;459:41–9.
32. Do K, Speranza G, Bishop R, Khin S, Rubinstein L, Kinders RJ, et al. Biomarker-driven phase 2 study of Mk-2206 and selumetinib (Azd6244, Arry-142886) in patients with colorectal cancer. Invest New Drugs 2015; 33:720–8.
33. Faller BA, Burtness B. Treatment of pancreatic cancer with epidermal growth factor receptor-targeted therapy. Biologics 2009;3:419–28.
34. Kindler HL, Richards DA, Garbo LE, Garon EB, Stephenson JJ Jr, Rocha-Lima CM, et al. A randomized, placebo-controlled phase 2 study of ganitumab (Amg 479) Or Conatumumab (Amg 655) in combination with gemcitabine in patients with metastatic pancreatic cancer. Ann Oncol 2012;23:2834–42.
35. Ko AH, Bekaii-Saab T, Van Ziffle J, Mirzoeva OM, Joseph NM, Talasaz A, et al. A multicenter, open-label phase ii clinical trial of combined mek plus egfr inhibition for chemotherapy-refractory advanced pancreatic adenocarcinoma. Clin Cancer Res 2015;22:61–9.
36. Weisner J, Landel I, Reintjes C, Uhlenbrock N, Trajkovic-Arsic M, Dienstbier N, et al. Preclinical efficacy of covalent-allosteric Akt inhibitor borussertib in combination with trametinib in kras-mutant pancreatic and colorectal cancer. Cancer Res 2019;79:2367–78.
37. Walters DM, Lindberg JM, Adair SJ, Newhook TE, Cowan CR, Stokes JB, et al. Inhibition of the growth of patient-derived pancreatic cancer xenografts with the Mek inhibitor trametinib is augmented by combined treatment with the epidermal growth factor receptor/her2 inhibitor lapatinib. Neoplasia 2013;15:143–55.
38. Kruspig B, Monteverde T, Neidler S, Hock A, Kerr E, Nixon C, et al. The Erbb network facilitates kras-driven lung tumorigenesis. Sci Transl Med 2018; 10.
39. Moll HP, Pranz K, Musteanu M, Grabner B, Hruschka N, Mohrherr J, et al. Afatinib restrains K-Ras-driven lung tumorigenesis. Sci Transl Med 2018;10.